Microstructure Study of Laser Surface Cladding of Bearing Materials

K. Chattopadhyay, S. Sanyal, G. Phanikumar,
Indian Institute of Science, Bangalore, INDIA
B.L. Mordike, R. Galun
IWW, TU-Clausthal, Clausthal Zellerfeld, Germany

1. Introduction

The present work investigates laser cladding as a technique to produce soft dispersion material on surface for bearing applications. Al-Si-Bi has been chosen as the dispersion material. Bismuth has liquid immiscibility with aluminium and forms a soft dispersion in a matrix of Al-Si alloy. Al-Si eutectic alloy was used as substrate due to its importance as a structural material. This work aims at microstructural characterization and understanding of microstructure development under different processing conditions. Microscopy is used to determine phase formation and size distribution of the dispersed phase. A model to understand the microstructure formation has been developed. The model involves simulation of laser melting to determine the temperature history of any location in the clad region and a microstructural model that involves nucleation, growth and coalescence of dispersion particles. We make an important conclusion that coalescence has a significant effect on the final size of the particles.

2. Experiments and analysis

Rofin Sinar R10000 Continuous wave CO_2 laser with peak power of 10kW is used for the cladding experiments. Elemental powders are mixed and fed into the laser melt pool to form the initial clad of required composition and thickness. The alloy clad is then remelted at various laser scan speeds to simulate different growth velocities. Transverse and longitudinal sections are taken from the laser clad/remelt samples for microstructure analysis.

Laser clad regions show fine eutectic microstructure of the clad and the remelt layers with a distribution of Bismuth particles. The remelted layer was distinguishable from the rest of the clad region, by the refinement in the microstructure. Fig. 1 shows the Al+12wt%Si+5wt% Bi alloy remelted at a laser scan speed of 2000 mm/min. Bi particles are in the interdendritic region. It can be seen that the particles are of two sizes. The larger ones are in the interdendritic region and the smaller ones within the dendrite. Remelting has given rise to an interesting feature of formation of network of Bi region (Fig. 2 a) and Bi seems to segregate in the inter dendritic regions (Fig. 2 b).

High magnification microstructures are used for particle size measurement. The particle size distribution thus obtained is an apparent size distribution due to stereological effects and has to be converted to real size distribution. We have converted this to a real distribution using a statistical analysis described by Saltykov [1]. Fig. 3 to Fig. 4 show such a size distribution. Here we note that most of the particles are of size less than a micrometer (0.5-1.0 μm) but there are few particles that are much larger (>5μm) indicating a bimodal distribution. The size of particles decreased from 0.5-1 μm to 0.3-0.4 μm as the remelt scan speed increased from 500 mm/min to 4000 mm/min. The mean distance between the particles also decreased from 12.3μm to 6.4μm.

Fig. 4 shows the apparent and corrected size distributions for the Al+12wt%Si+10wt%Bi samples remelt at various speeds. The size intervals are chosen to conform more closely to the requirement of Saltykov analysis. Since the number of particles is not large, the bimodal distribution is not as discernible as for the 5wt%Bi samples. However, it can be noticed that there are two sizes of

particles. We could summarize the experimental observations that the Al-Si-Bi alloys remelted at various speeds show a fine dispersion of Bi particles in bimodal distribution and form networks at the bottom of the pool for higher concentration.

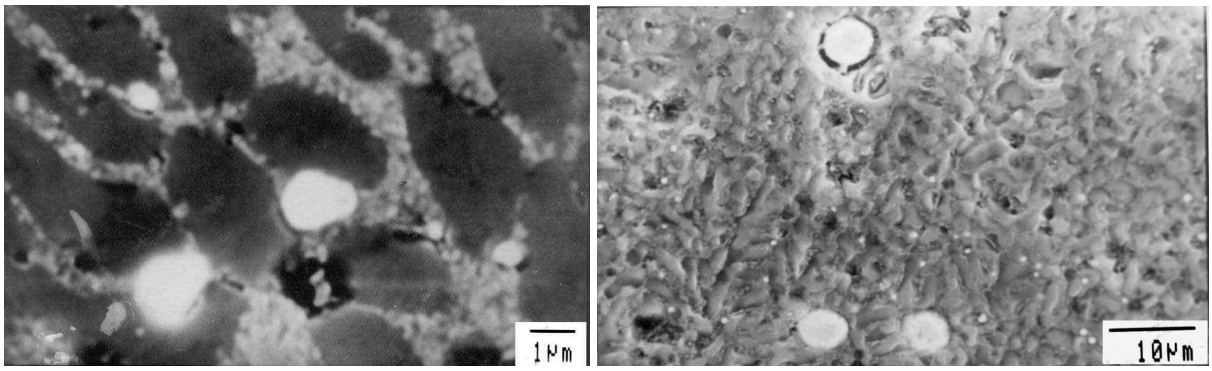

Fig. 1: SEM of alloy remelt at 2000 mm/min showing two sizes of particles.

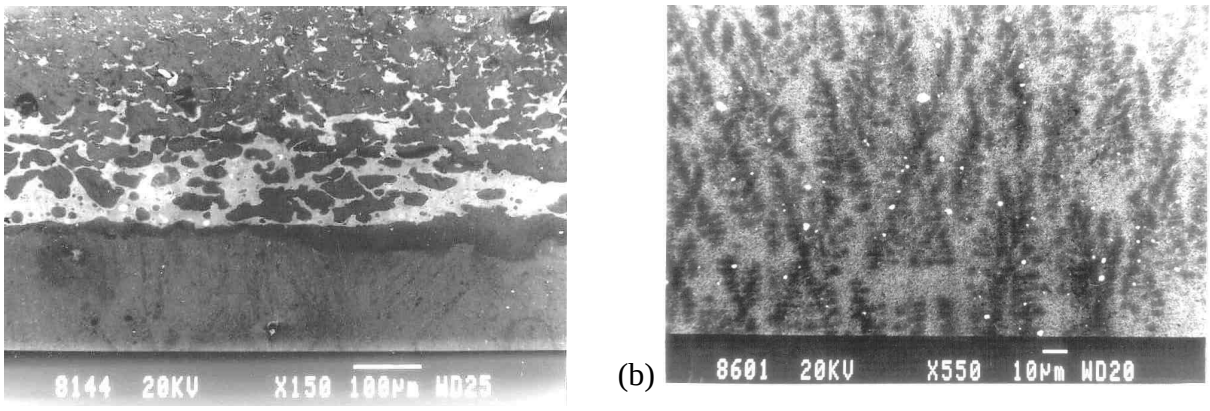

(a) (b)

Fig. 2: Microstructures of the alloy clad at 150 mm/min and remelt at 900mm/min (a) Network formation at the bottom of the pool (b) Bi particles along the dendrite boundaries.

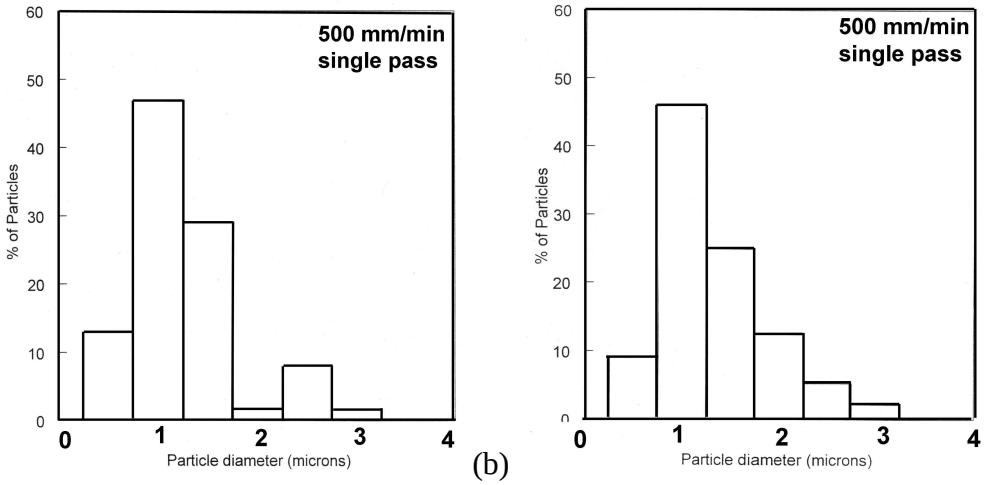

(a) (b)

Fig. 3: Bi particle size distribution in Al+12wt%Si+5wt%Bi remelted at 500mm/min. (a)apparent size distribution (b)corrected size distribution

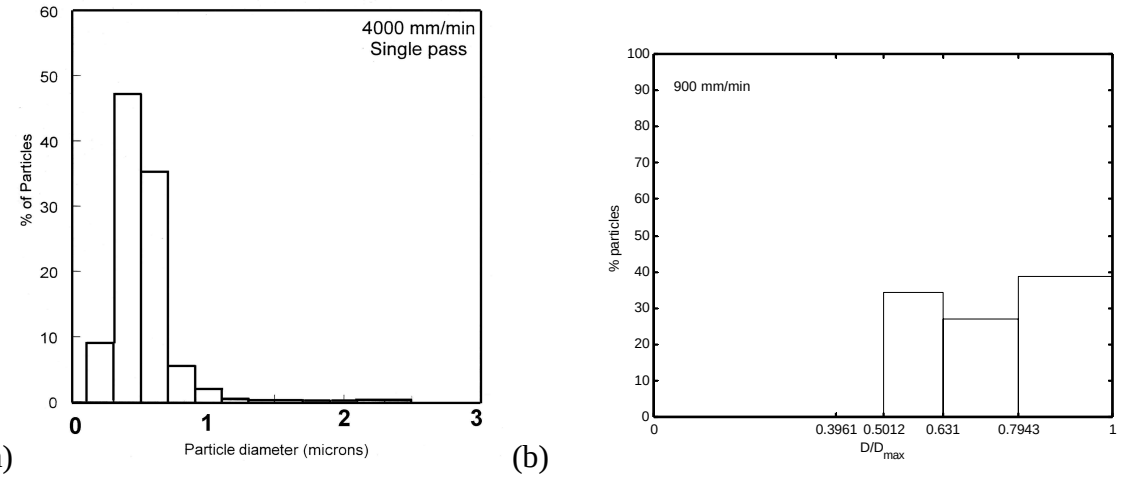

(a) (b)

Fig. 4: Bi particle size distribution in (a)Al+12wt%Si+5wt%Bi remelted at (a)4000mm/min. (b)Distribution for Al+12wt%Si+10wt%Bi clad at 150mm/min and remelt at 600mm/min.

3. Modeling and results

The process of microstructural evolution in laser cladding could be visualized in two stages. At the macro level, the laser melting with heat transfer and fluid flow dictates the size and shape of the liquid zone. The temperature history of various locations in the clad region is given by the solution of the laser melting problem. At the micro level, the microstructure is determined by the nucleation, growth, coarsening and coalescence of the soft dispersion phase in the clad pool. These processes are determined by the temperature history. Thus, we have an option of modeling the problem in two stages, to arrive at the final aim of microstructure in terms of size distribution of the dispersed phase.

3.1 Laser Melting

The laser melting process involves a continuous-beam laser moving with a constant scanning speed, u_{scan}, along the x-direction. Since the molten pool moves with the laser beam, the problem is more conveniently studied in a reference frame fixed with the laser. Although a final quasi-steady state will be reached, our formulation is transient to predict the evolution of pool development and obtain temperature history of any location in the domain. The fundamental variables solved for are temperature (T) and velocity of liquid in the laser melt pool (u,v,w). The governing equations for the process are given below.

Continuity: $$\frac{\partial r}{\partial t}+\nabla\cdot\left(r\vec{u}\right)=0$$

X-momentum: $$\frac{\partial}{\partial t}\left(ru\right)+\nabla\cdot\left(r\vec{u}u\right)=\nabla\cdot\left(m\nabla u\right)-\frac{\partial p}{\partial x}-\left(\frac{K\left(1-e\right)^2}{e^3+b}\right)u-\frac{\partial}{\partial x}\left(ru_{scan}u\right)$$

Y-momentum: $$\frac{\partial}{\partial t}\left(rv\right)+\nabla\cdot\left(r\vec{u}v\right)=\nabla\cdot\left(m\nabla v\right)-\frac{\partial p}{\partial y}-\left(\frac{K\left(1-e\right)^2}{e^3+b}\right)v+rgb_T\left(T-T_r\right)-\frac{\partial}{\partial x}\left(ru_{scan}v\right)$$

Z-momentum: $$\frac{\partial}{\partial t}\left(rw\right)+\nabla\cdot\left(r\vec{u}w\right)=\nabla\cdot\left(m\nabla w\right)-\frac{\partial p}{\partial z}-\left(\frac{K\left(1-e\right)^2}{e^3+b}\right)w-\frac{\partial}{\partial x}\left(ru_{scan}w\right)$$

Energy conservation: $$\frac{\partial}{\partial t}\left(rH\right)+\nabla\cdot\left(r\vec{u}H\right)=\nabla\cdot\left(k\nabla T\right)-\frac{\partial}{\partial t}\left(r\Delta H\right)-\frac{\partial}{\partial x}\left(ru_{scan}H\right)$$

where, ρ is the density, u_{scan} is the laser scan velocity, μ is the viscosity, g is acceleration due to gravity, β_T is the compressibility constant, x-y-z are the co-ordinate axes. The enthalpy, *H*, of a material can be expressed as $H = cT + f_L L$, where *c* is specific heat, *L* is latent heat, f_l is liquid fraction. In the present problem, the substrate is eutectic Al-Si, hence a pure metal melting and solidification should suffice. A gaussian heat source was applied at the top of the work piece. Marangoni flow at the top of the liquid pool and convective losses at all walls are taken in to consideration. Further details of formulation are given elsewhere [2,13].

The governing equations are solved under the respective boundary conditions simultaneously using a control volume technique. SIMPLER procedure [3] with tri-diagonal-matrix algorithm is used for the solution. The results of modeling of laser melting are shown in the temperature and fluid flow of the laser melt pool as a snap shot at any instant. Fig. 5 shows the temperature and velocity distribution in the melt pool. The melt pool is shallow, as desirable for cladding, due to marangoni dominated radial outward flow. The maximum velocity is on the top of the pool near the solid-liquid interface and about 3m/s in magnitude. The calculations are transient and so we can obtain the temperature history of any location in the melt pool. The temperature history of a point at the center of the pool is shown in the Fig. 6. In the zoomed plot, we can see the time intervals allowed for nucleation and diffusional growth calculated from the corresponding temperature intervals. For the present case of Al+1.414at% Bi, these intervals are evaluated as described in the next section.

3.2 Nucleation of Bi particles

Nucleation of second phase in the liquid immiscible systems can be adequately described by homogeneous nucleation theory as shown by Granasy and Ratke [4]. A thermodynamic description of the binary system Al-Bi is required to arrive at the driving force for nucleation of the Bi particles. The free energy of Al-Bi system, for the temperature range (930K to 1310K) within which immiscibility exists, is given by a subregular solution model [5]. The systems Al-Si-Bi and Al-Bi studied by Ratke et al [6,7] show similar features. To reduce complexity of the problem, we have chosen to consider only Al-Bi system for all our calculations.

The free energy expression used is:

$$\Delta G = \sum_{i=0}^{n} K_i x_1 x_2 (x_1 - x_2)^i - RT\left(x_1 \log x_1 + x_2 \log x_2\right)$$

Where, $K_0 = 24649.18 - 3.04970T$, $K_1 = 13282.64 - 5.92753T$, $K_2 = 18519.75 - 12.33873T$, and $K_3 = 6959.30 - 2.24613T$. All K_i are in J/mol.

The free energy vs. composition curve for any given temperature is used to arrive at the driving force for phase separation as illustrated by Thompson and Spaepen [8]. The surface energy of a critical system such as the immiscible liquid system Al-Bi is described by the relation [9] $s = s_O (1 - T/T_C)^{1.26}$, where s_O is a constant. s is taken to be 0.06 J/m^2 at the monotectic temperature [10]. Homogeneous nucleation rate for phase separation is given by $I = I_O \exp\left(-\Delta G^* / k_B T\right)$ where $\Delta G^* = (16 p s^3)/(3\Delta G_V^2)$ and ΔG_V is the volume free energy. The pre-exponent factor I_o was evaluated using the classical expression for nucleation rate [4]. $I_0 = N_0 O \Gamma Z \exp(-\Delta G^* / kT)$, where, N_0 is the number density of atoms in the liquid, $O = 4n^{2/3}$, *n* is the number of atoms in the droplet of critical size, $\Gamma = 6D / l^2$, l is the average jump distance of atoms in the liquid, and *D* is the diffusivity.

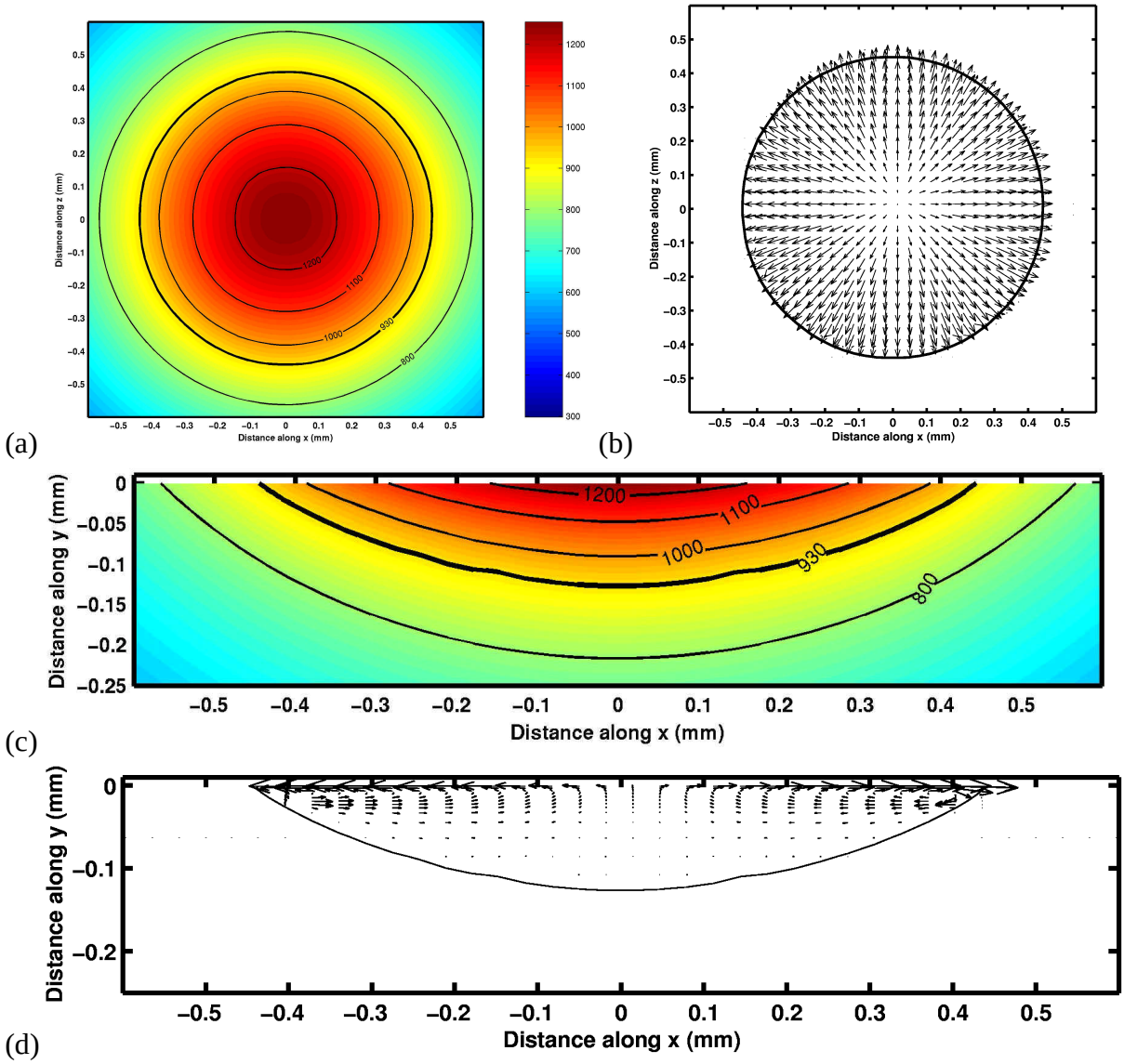

Fig. 5: (a)Top view of temperature distribution. (b)velocity profile on the top surface. Cross-section view of (c) temperature distribution. (d)velocity profile. Contour labels are in kelvin

The critical radius of the nucleus is given by $R^* = 2s / \Delta G_V$ [11]. The undercooling that takes place before phase separation occurs is given by the minimum in R^*. Nucleation rate calculated using the above expression is shown in the Fig. 7(a). A plot of R^* with temperature is shown for Al+10wt%Bi in Fig. 7(b). The thin line on the right indicates the equilibrium liquidus temperature. It can be seen that an undercooling of about 25K is possible. The dotted lines in Fig. 7(a) show the temperature range for nucleation calculation where the critical radius is small. The time interval spent by any point in the laser melt pool within this temperature range is what is used for nucleation number calculation.

3.3 Growth of Bi particles

Growth of Bi particles takes place via diffusion [12] and LSW coarsening [11]. The time scale for these processes to take place is of the order of 10^{-3}s for the laser processing technique used in this project. An order of magnitude analysis is performed to determine the dominant of the two processes.

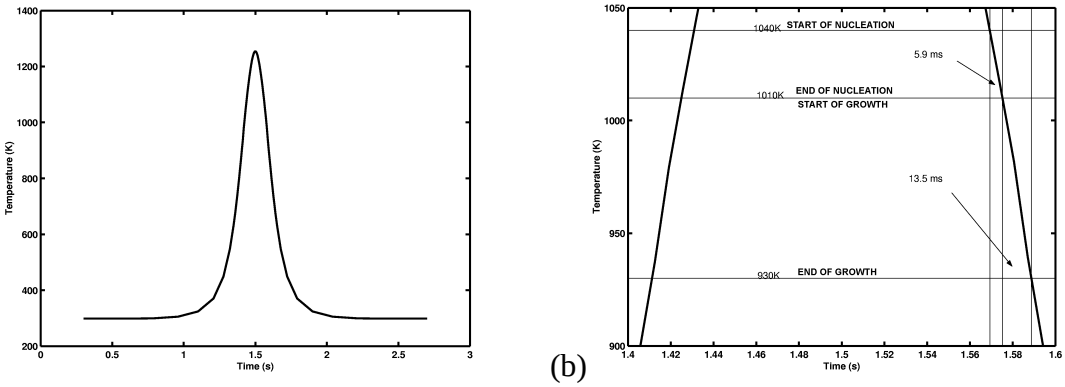

(a) (b)

Fig. 6: (a)Temperature history of a point at the center of pool. (b)Time intervals available for nucleation and growth.

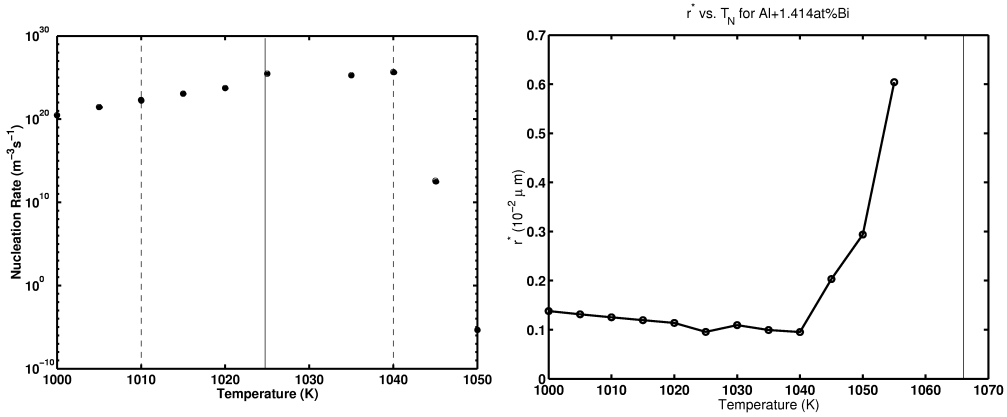

Fig. 7: (a)Plot of nucleation rate with temperature. The thin line corresponds to the temperature at which the critical nucleus radius is the smallest. The dashed lines show the temperature interval used for nucleation. (b) Plot of critical radius with nucleation temperature for Al+1.414at%Bi.

The transport constant for LSW coarsening [11] is given by $K_{LSW} = (8s\Omega C_\infty D)/(9k_B T\Delta C)$. At T=1030K, $K_{LSW} \approx 4\times10^{-19} m^3 s^{-1}$. The size of particles after growth is given by $\Delta R \approx \sqrt{2D\Delta t a}$ where, a is the supersaturation. Diffusivity was estimated using Stokes-Einstein equation at the same temperature: $D = k_B T(3\pi a_o h)^{-1} \approx 4.7\times10^{-9} m^2 s^{-1}$. It can be seen that diffusional growth of particles in the liquid for the time scale involved (~5ms) gives almost two orders higher value than coarsening. Hence, we have neglected LSW coarsening in our calculations. However, for long time scales and lower temperatures, this could be of importance.

Growth by diffusion can take place only till the supersaturation is exhausted. Growth of a particle at the center of the pool is shown in Fig. 8(a). This will be the starting size for the collision and coalescence calculation to obtain final size distribution. The time interval allowed for collision and coalescence is the same as the maximum allowed time interval for growth as shown in Fig. 6.

3.4 Collision and coalescence of particles

The nucleation and growth of the particles takes place in a liquid pool that undergoes vigorous convection driven by marangoni forces [13]. It is clear that coalescence due to collision of particles

will be present during the process. Sedimentation is negligible as the velocities for convection in laser melt pool are large (of the order of 1m/s) and thus, significantly higher than stokes velocities. The size of the particle after diffusional growth for the time scale and temperatures involved during the solidification stage of the laser cladding process is shown in Fig. 8 (a), for a particle at the center of the clad region. The experimentally observed sizes are about 10 times larger. Thus the need to take coalescence by collision in to account.

Coagulation and coalescence of particles under motion is well studied and a review by Drake [14]. However, not much literature exists for coalescence of particles during solidification [11]. The models discussed by Drake and Ratke involve collision frequency as a function of velocity of the particles. This term is nearly impossible to evaluate for laser melting process for which, the velocity profile is solved numerically as a function of position, time and process conditions. Thus, we have resorted to a method outlined below to take coalescence in to account. We make the following assumptions:

- Particles move along with the liquid and the drag due to difference in density is negligible.
- Particles are small enough in volume fraction (<0.1) that they have no effect on the liquid flow profile.
- Particles that have undergone diffusional growth are taken for coalescence study during which they only collide and coalesce but do not grow. Growth and coalescence can be treated as discrete steps in the process for simplicity and as a first approximation.

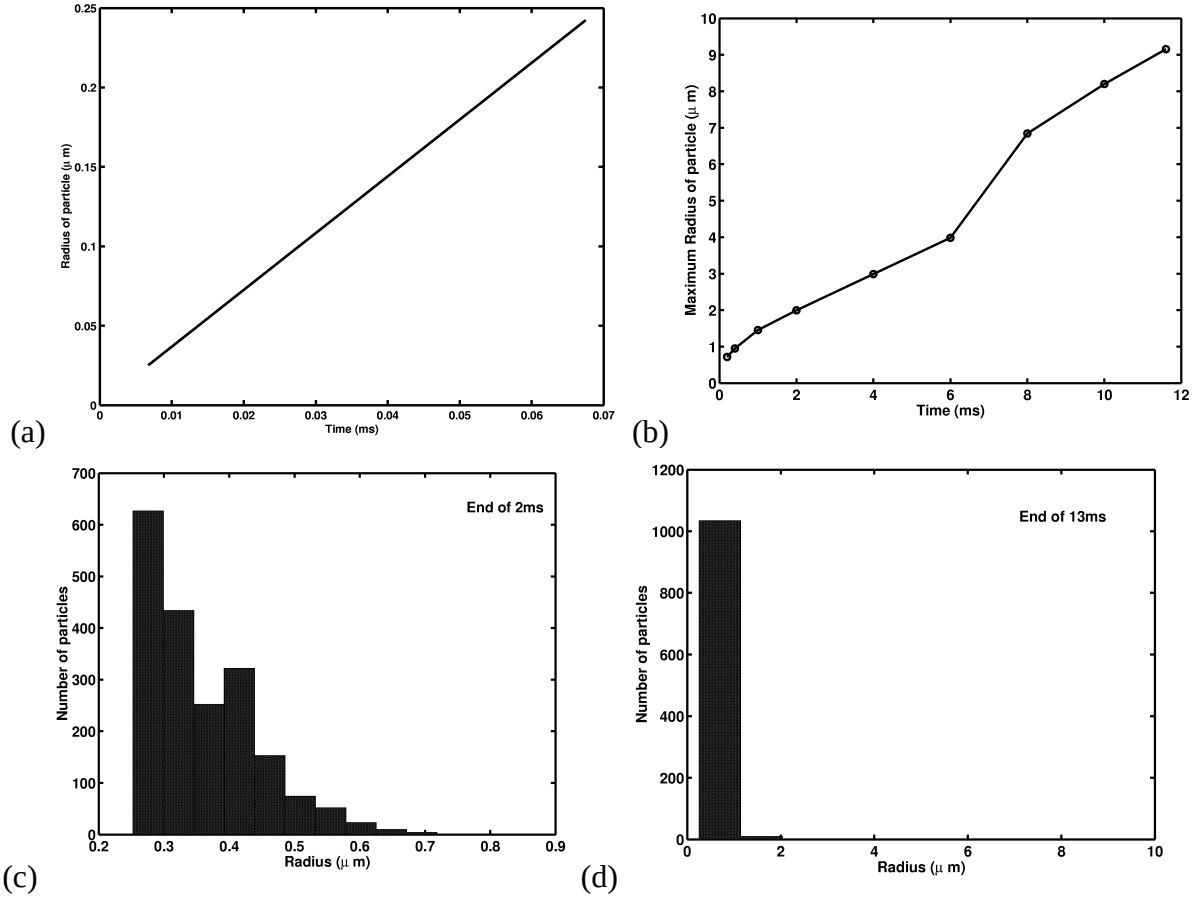

Fig. 8: (a) Growth of a particle evaluated till the supersaturation is exhausted. (b) Variation of maximum size of particle with time of convection. Particle size evolution during collision and coalescence. (c)Initial stage, after 2ms (d)Final stage,after 13ms.

Particles of sizes after diffusional growth and in a number proportional to the nucleation rate are taken and introduced in the laser melt pool at various time steps. The locations of particles within the clad region are chosen by random number generation. A number of particles (64000) are introduced in to a small volume in the melt pool such that it corresponds to the average nucleation sites in that volume for the time interval of nucleation. The particles are then traced by integrating the fluid velocities at the respective locations using a Runge-Kutta method of order 4. Two particles (labeled 1,2) are joined and the size of #1 increased for volume conservation when they come close enough by the following criterion: $\left|(x_1 - x_2)^2 + (y_1 - y_2)^2 + (z_1 - z_2)^2\right| \le (r_1 + r_2)^2$, where ($x_1$,$y_1$,$z_1$) and ($x_2$,$y_2$,$z_2$) are positions of the two particles with radii r_1 and r_2, respectively.

Fig. 8 shows the particle size evolution with time. The maximum size of particle at any stage of coalescence is shown in Fig. 8 (c). It can be seen that the size of particles increases by almost an order of magnitude due to collision and coalescence. The histograms in Fig. 8 (c,d) show that most of the particles are on the lower end of the size range spectrum. The total number of particles keeps fluctuating as the coalescence takes place. Features such as fine time steps, large number of particles, tracing and searching particles for coalescence render this stage of calculation cpu-intensive. A large number of calculations of this kind are to be performed for various scan speeds to make a statistical study and gain further insight in to the coalescence process.

4. Conclusions

Laser surface cladding of bearing material Al-Si-Bi has been successfully done to produce a fine dispersion of soft Bi particles in Al-Si matrix. The size distribution of Bi particles is bimodal. Computational model of the process is developed to estimate realistic temperature profile of the process. Size of particles after growth is too small in comparision with the experimentally observed one. Coalescence is shown as the significant factor in the final size of particles.

5. References

(1) Erwine E. Underwood, *Quantitative Stereology*, (1970).

(2)G. Phanikumar et. al., *Int. J. for Num. Methods in Heat and Fluid Flow*, 11(2001) pp 156-171.

(3) S.V. Patankar, *Numerical Heat Transfer and Fluid Flow*, Hemisphere Publications, New York (1980), 2nd ed.

(4) L. Granasy and L. Ratke, *Scripta Metallurgica et Materialia*, 28 (1993), pp.1329-1334.

(5) Private Comm., F. Sommer, MPI, Stuttgart. Courtesy, L. Ratke, DLR, Cologne, Germany.

(6) H. Ahlborn, S. Diefenbach, H. Neumann, B. Prinz, L. Ratke, A. Romero, *Mat. Sc. and Engineering*, A173 (1993), pp.133-135.

(7) Jens Alkemper and Lorenz Ratke, *Z. Metallkunde*, 85 (1994), pp.365-371.

(8) C.V. Thompson and F. Spaepen, *Acta Metallurgica*, 31 (1983), pp.2021-2027.

(9) Fritz Falk, *Immiscible liquid metals and organics*, Ed. L. Ratke, DGM Informationsgesselshaft mbH (1993) Oberursel, Germany, pp.93-100.

(10) B. Derby and J.Favier, *Acta Metallurgica*, 31 (1983), pp. 1123-1130.

(11) L. Ratke, S. Diefenbach, *Materials Science and Engineering*, R15 (1995) pp.263-347.

(12) C. Zener, *Journal of Applied Physics*, 20 (1949), pp.950-953.

(13) P.Mohanraj, S.Sarkar, S.Chakraborty, G.Phanikumar, P.Dutta, and K.Chattopadhyay, *Advances in Computational Heat Transfer*, CHT'01, May20-25, Queensland, Australia (2001), (to appear in International Journal of Heat and Fluid Flow).

(14) R.L. Drake, in *Topics in Aerosol Research*, (G.M. Hidy and J.R. Brock, Eds.), 2 (1970) pp.203, Pergamon, New York, 1970.